

Searches for stochastic gravitational-wave backgrounds

Joseph D. Romano

Les Houches Summer School
July 2018

Abstract

These lecture notes provide a brief introduction to detection methods used to search for a stochastic background of gravitational radiation—i.e., a superposition of gravitational-wave signals that are too weak or too numerous to individually detect. The lectures are divided into two main pieces: (i) an overview, consisting of a description of different types of gravitational-wave backgrounds and an introduction to the correlation method using multiple detectors; (ii) details, extending the previous discussion to non-trivial detector response, what to do in the absence of correlations, and a recently proposed Bayesian method to search for the gravitational-wave background produced by stellar-mass binary black hole mergers throughout the universe. Suggested exercises for the reader are given throughout the text.

Contents

1 Motivation	3
1.1 Gravitational-wave analogue of the cosmic microwave background	3
1.2 The background of BBH and BNS mergers in the LIGO band	4
2 Different types of stochastic backgrounds	5
2.1 Different sources	5
2.2 Different signal properties	6
3 Mathematical characterization of a stochastic background	9
3.1 Plane-wave expansion	9
3.2 Ensemble averages	10
3.3 Energy density spectrum in gravitational waves	11
3.4 Calculating $\Omega_{\text{gw}}(f)$ for an astrophysically-generated background	12
3.4.1 Example: $\Omega_{\text{gw}}(f)$ for binary inspiral	12
4 Correlation methods	14
4.1 Basic idea	14
4.2 Extension to multiple data samples	15
4.3 Optimal filtering	16
5 Optimal filtering applied to some simple examples	17
5.1 Single-component analyses	17
5.2 Multi-component analysis	19
6 Non-trivial detector response	19
7 Non-trivial correlations	19
8 What to do in the absence of correlations?	19
9 Searching for the background of binary black-hole mergers	19
10 Exercises	20

1 Motivation

A stochastic background of gravitational radiation is a superposition of gravitational-wave signals that are too weak or too numerous to individually detect. The individual signals making up the background are thus *unresolvable*, unlike the large signal-to-noise binary black-hole (BBH) and binary neutron-star (BNS) merger signals recently detected by the advanced LIGO and Virgo detectors. But despite the fact that the individual signals are unresolvable, the detection of a stochastic gravitational-wave background (GWB) will be able to provide information about the *statistical* properties of the source.

1.1 Gravitational-wave analogue of the cosmic microwave background

The ultimate goal of gravitational-wave background searches is to produce the GW analogue of Figure 1, which is a sky map of the temperature fluctuations in the cosmic microwave background

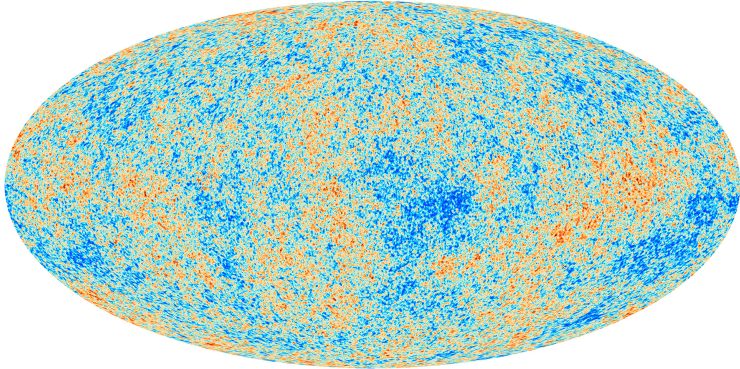


Figure 1: Skymap of $\Delta T/T_0$ for the cosmic microwave background radiation produced by the Planck 2013 mission.

(CMB) blackbody radiation, $\Delta T/T$, relative to the $T_0 = 2.73$ K isotropic component. (The dipole contribution due to our motion with respect to the cosmic rest frame has also been subtracted out.) Recall that the CMB is a background of electromagnetic radiation, produced at the time of last scattering, roughly 380,000 yr after the Big Bang. At that time, the universe had a temperature of ~ 3000 K, approximately one thousand times larger than the temperature today, but cool enough for neutral hydrogen atoms to first form and photons to propagate freely. The temperature fluctuations in the CMB radiation tell us about the density of matter on the surface of last scattering, thus giving us a picture of the “seeds” of large-scale structure formation in the early universe. Given the weakness of the gravitational interaction compared to the electromagnetic force, the GW analogue of Figure 1 would give us a picture of the Universe a mere fraction of a second after the Big Bang (this is explained in a bit more detail in Section 2.1)—a “holy grail” for gravitational-wave astronomy.

For perspective, Figure 1 was produced by the Planck mission in 2013, almost 50 years after the CMB radiation was initially detected by Penzias and Wilson in 1965. It took many years and improved experiments (COBE, Boomerang, WMAP, Planck to name a few) to get to the high-precision measurements that we have today. So it is somewhat sobering to realize that now—at the end of 2018—we have yet to detect the isotropic component of the GWB.

1.2 The background of BBH and BNS mergers in the LIGO band

Fortunately, as mentioned above, the advanced LIGO and Virgo detectors have detected other gravitational-wave signals from several individual BBH and BNS mergers. These were very strong signals, having matched-filter signal-to-noise ratios $\text{SNR} \gtrsim 10$, and false alarm probabilities $< 2 \times 10^{-7}$, corresponding to 5-sigma “gold-plated” events. Similar large SNR detections are expected during the upcoming observing run O3, which is scheduled to start in early 2019. But we also expect that there are many more signals, corresponding to more distant mergers or smaller mass systems, which are individually undetectable (i.e., *subthreshold* events). This weaker background of gravitational radiation is nonetheless detectable *as a collectivity* via the common influence of the gravitational waves on multiple detectors.

To get an idea of the statistical properties of this background signal, we can estimate the total rate of stellar-mass BBH mergers throughout the universe by using the local rate estimate from these first detections, $9\text{--}240 \text{ Gpc}^{-3} \text{ yr}^{-1}$. This leads to a prediction for the total rate of BBH mergers between ~ 1 per minute to a few per hour. (You are asked in Exercise 1 to verify these predictions.)¹ Since the duration of BBH merger signals in band is ~ 1 s, which is much smaller than the average duration between successive mergers, the combined signal will be highly-nonstationary (or *popcorn-like*). We can perform similar calculations for BNS mergers. The predicted total rate for such events is roughly one event every 15 s, while the duration of a BNS signal in band is roughly 100 s. Thus, the BNS merger signals overlap in time leading to a continuous (or *confusion-limited*) background. Figure 2 is a plot of the expected time-domain signal corresponding the rate estimates calculated above.

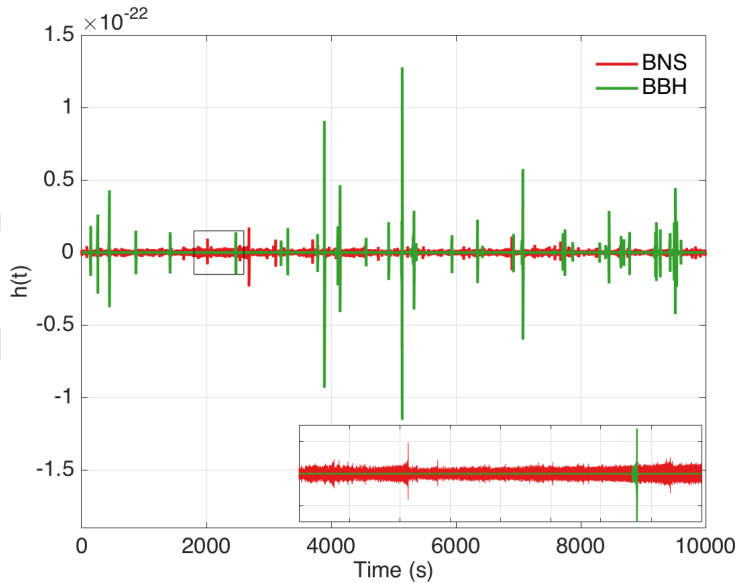


Figure 2: Simulated time-domain signal for the predicted BBH and BNS background. Figure taken from [?].

The combined signal from BBH and BNS mergers is potentially detectable with advanced LIGO and Virgo, shortly after reaching design sensitivity. Although the signal-to-noise ratios for

¹A more complete description of this and all other exercises are given in Section 10. The number next to “Exercise” is a link that brings you to the detailed exercise in Section 10.

the individual events are small, the combined signal-to-noise ratio of the correlated data summed over all events grows like the square-root of the observation time, reaching a detectable level of 3-sigma after roughly 40 months of observation (Figure 3). This estimate of time to detection is

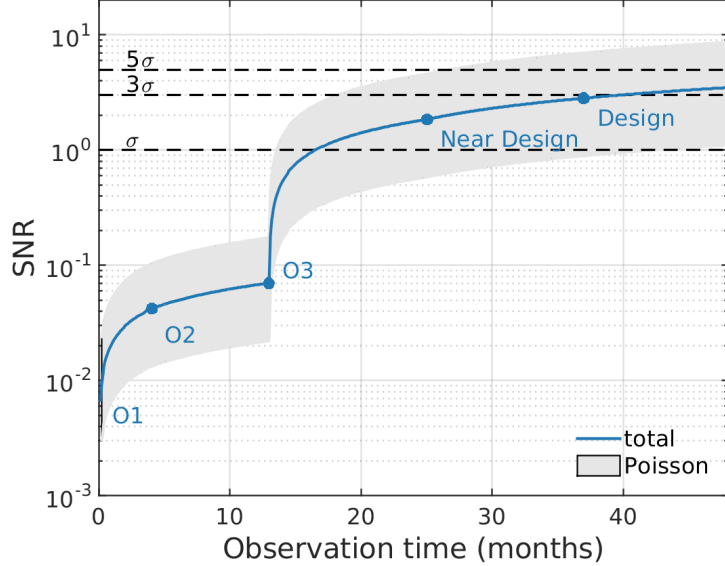


Figure 3: Expected signal-to-noise ratio of the correlated data for the advanced LIGO and Virgo detectors as a function of observation time. The points labeled O1, O2, etc., indicate the start of advanced LIGO’s first observation run, second observation run, etc. Figure taken from [?].

based on the standard cross-correlation search (Section 4), which assumes a Gaussian-stationary background. But there is a better method, recently proposed by Smith and Thrane [3], which should reduce the time to detection by several orders of magnitude (factor of ~ 1000), meaning that the background would be detectable after only a few days of operation. We will describe this method in more detail in Section 9.

2 Different types of stochastic backgrounds

2.1 Different sources

The combined signal from stellar-mass BBH and BNS mergers throughout the universe is just one way of producing a GWB. Due to the relatively small masses of stellar-mass BHs and NSs, the signal is at the high-frequency end of the spectrum (~ 10 Hz to a few kHz), which is the sensitive band for the current generation of km-scale ground-based laser interferometers like LIGO and Virgo. Heavier-mass systems, which produce lower-frequency gravitational waves, are also expected to give rise to GWBs that are potentially detectable with other existing or proposed detectors. Figure 4 is a plot of the gravitational-wave spectrum, with frequencies ranging from a few kHz (for ground-based detectors) to 10^{-17} Hz (corresponding to a period equal to the age of the universe), together with potential sources of GWBs and relevant detectors.

Of particular note is the combined gravitational-wave signal produced by compact white-dwarf binaries in the Milky Way, producing a “confusion-limited” GWB in the frequency band $\sim 10^{-4}$ Hz to 10^{-1} Hz. This is a guaranteed signal for the proposed space-based interferometer LISA, which

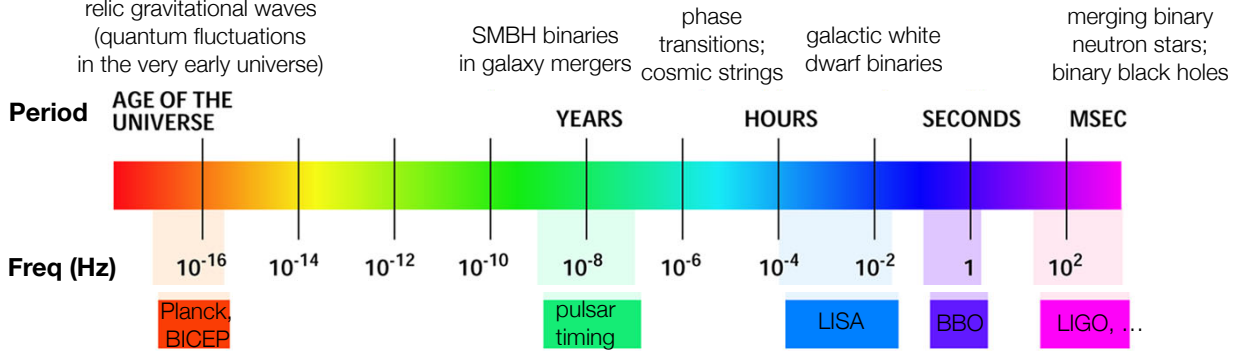


Figure 4: Detectors and potential sources of gravitational-wave backgrounds across the gravitational-wave spectrum.

consists of three spacecraft (each housing two lasers, two telescopes, and two test masses) in an equilateral-triangle configuration (arm lengths of several million km) in orbit around the Sun (expected launch date 2034). The signal is expected to be so strong that it will dominate the instrumental noise at low frequencies, forming a gravitational-wave ‘foreground’ that will have to be contended with when searching for other gravitational sources in the LISA band.

At lower frequencies between $\sim 10^{-9}$ Hz and 10^{-7} Hz (corresponding to periods of order decades to years), pulsar timing arrays can be used to search for the GWB produced by the inspiral and merger of supermassive black-holes (SMBHs) in the centers of distant galaxies. A pulsar timing array basically functions as a galactic-scale gravitational-wave detector, with the radio pulses emitted by each pulsar behaving like ‘ticks’ of an extremely stable clock. By carefully monitoring the arrival times of these pulses, one can search for a GWB by looking for correlated modulations in the arrival times induced by a passing gravitational wave.

In addition to these *astrophysical* GWBs associated with stellar-mass or supermassive BHs and NSs, one also expects backgrounds of *cosmological* origin, produced in the very early universe, much before the formation of stars and galaxies. Two examples, indicated in Figure 4, are cosmic strings (line-like defects associated with phase transistions in the early universe) and relic gravitational waves (quantum fluctuations in the geometry of space-time, driven to macroscopic scales by a period of rapid expansion—e.g., inflation—a mere $\sim 10^{-32}$ s after the Big Bang). This relic background is potentially detectable by its effect on the polarization of the CMB radiation. The Planck satellite and BICEP experiment (located at the South Pole) are searching for this signal.

2.2 Different signal properties

Not surprisingly, different sources of a GWB give rise, in general, to different properties of the observed signal. These differences are what will allow us to infer the source of the background from the measured signal. For example:

(i) Stochastic backgrounds can differ from one another in terms of the angular distribution of gravitational-wave power on the sky. Cosmologically-generated backgrounds, like those from cosmic strings or relic gravitational waves, are expected to be statistically *isotropic*, with equal gravitational-wave power in all different directions, similar to the CMB (Figure 1). Different statistically isotropic backgrounds will be characterized by different angular power spectra, C_l as a

function of multipole moment l , where

$$C(\theta) = \sum_{l=0}^{\infty} \frac{2l+1}{4\pi} C_l P_l(\cos \theta), \quad (2.1)$$

is the angular correlation between the gravitational-wave power coming from two directions \hat{n} and \hat{n}' separated by angle θ . Statistically isotropic backgrounds are to be contrasted with *anisotropic* backgrounds, whose distribution of power on the sky follows the spatial distribution of sources. For example, the “confusion-limited” foreground that LISA will see from the population of close white-dwarf binaries in the Milky Way will have its gravitational-wave power concentrated in the direction of the Milky Way. Figure 5 shows simulated skymaps for a statistically isotropic background (left panel) and an anisotropic background (right panel). The anisotropic background in that figure follows the galactic plane in equatorial coordinates.

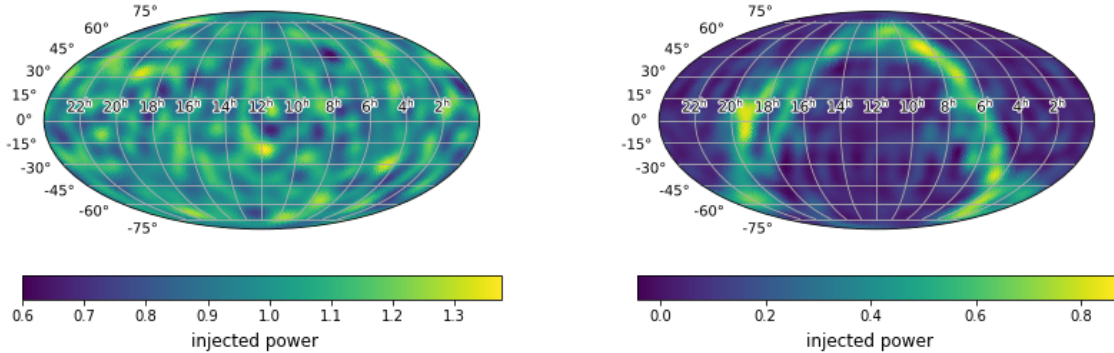


Figure 5: Simulated sky maps of gravitational-wave power for a statistically isotropic background (left panel) and an anisotropic background (right panel).

(ii) Stochastic backgrounds can also differ in temporal distribution and amplitude. We have already seen examples of this in Figure 2, for the expected backgrounds from stellar-mass BBH mergers and BNS mergers throughout the universe (a LIGO source). As mentioned earlier, the rate estimates and durations of these individual merger signals are such that the BBH background is expected to be popcorn-like (consisting of non-overlapping mergers), while that for the BNS background is expected to be stationary and confusion-limited (consisting of several overlapping BNS mergers at any instant of time). Another example of non-trivial temporal dependence is the confusion-limited signal from close white-dwarf binaries in the Milky Way (a LISA source). This is an amplitude-modulated signal with a 6-month period (Figure 6), due to LISA’s “cartwheeling” orbital motion around the Sun. (The antenna pattern of LISA will point in the direction of the Galactic center twice every year.) From the figure, we also see that the expected white-dwarf binary signal will be larger than that of the instrumental noise for LISA, thus constituting an astrophysical *foreground*. This is atypical, however, as most expected GWBs will sit below the instrumental noise (e.g., for advanced LIGO / Virgo, pulsar timing, CMB polarization experiments), requiring observation over long periods of time to confidently detect.

(iii) Stochastic backgrounds can also differ in their power spectra as shown in Figure 7. Here we plot simulated time-domain data (including the signals for an individual BNS merger and BBH ringdown²), histograms, and power spectra for three different types of GWBs. For these toy-model

²Our toy-model simulation for BBH ringdown is simply a damped sinusoid with frequency 440 Hz. It has the correct qualitative behavior for a BBH ringdown, but is not meant to be astrophysically realistic.

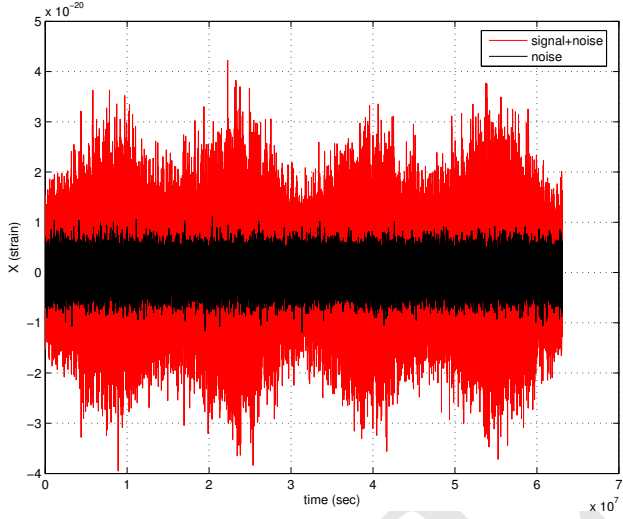


Figure 6: Simulated time-domain output of a particular combination of the LISA data over a 2-year period. The modulation of the signal with a 6-month period is apparent in the data. Figure taken from [2].

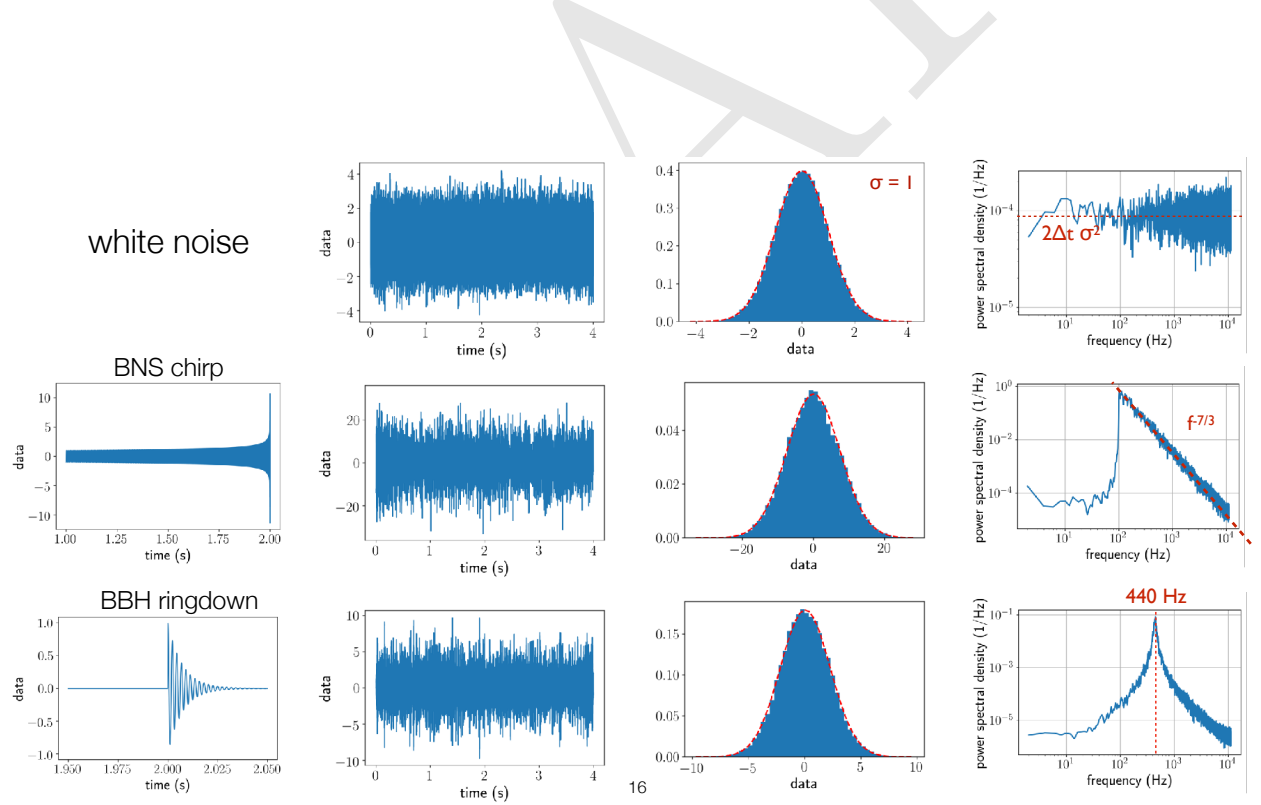


Figure 7: Simulated time-domain data (including the signals for an individual BNS merger and BBH ringdown), histograms, and power spectra for three different types of Gaussian-stationary GWBs.

simulations, we overlapped a sufficient number of individual BNS merger and BBH ringdown signals to produce Gaussian-stationary confusion-limited GWBs (second column and third columns). The difference between these backgrounds shows up in their power spectra (third column). The power spectra for the BNS merger and BBH ringdown backgrounds have the same shape as those for an individual BNS merger or BBH ringdown, scaled by the total number of sources contributing to the background.

3 Mathematical characterization of a stochastic background

Since the individual signals comprising a GWB background are either too weak or too numerous to individually detect, the combined signal for the background is for all practical purposes *random*, similar to noise in a single detector. Hence, we need to describe the GWB *statistically*, in terms of moments (i.e., ensemble averages) of the metric perturbations describing the GWB.

3.1 Plane-wave expansion

Recall that gravitational waves are time-varying perturbations to the geometry of space-time, which propagate away from the source at the speed of light. In transverse-traceless coordinates $(t, \vec{x}) \equiv (t, x^a)$, where $a = 1, 2, 3$, the metric perturbations corresponding to a plane wave (propagating in direction $\hat{k} \equiv -\hat{n}$) have two degrees of freedom, corresponding to the amplitudes of the plus (+) and cross (\times) polarizations of the gravitational wave (Figure 8). The metric perturbation for the

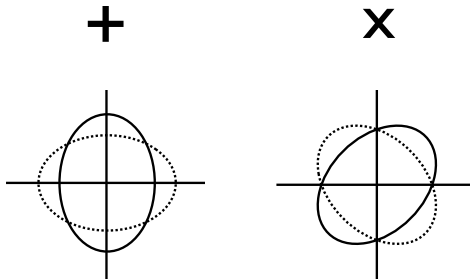


Figure 8: The two orthogonal polarizations of a gravitational wave. A circular ring of test particles in the plane orthogonal to the direction of propagation of the wave are alternately deformed into ellipses, as space is “squeezed” and “stretched” by the passing of the wave.

most general GWB can thus be written as a superposition of such wave:

$$h_{ab}(t, \vec{x}) = \int_{-\infty}^{\infty} df \int d^2\Omega_{\hat{n}} \sum_{A=+, \times} h_A(f, \hat{n}) e_{ab}^A(\hat{n}) e^{i2\pi f(t + \hat{n} \cdot \vec{x}/c)} \quad (3.1)$$

where f denotes the frequency of the component waves, \hat{n} their direction on the sky, and $A = +, \times$ their polarization. (The direction of propagation of the component waves is given by $\hat{k} = -\hat{n}$.) The quantities $e_{ab}^A(\hat{n})$ are polarization tensors, given by

$$\begin{aligned} e_{ab}^+(\hat{n}) &= \hat{l}_a \hat{l}_b - \hat{m}_a \hat{m}_b, \\ e_{ab}^\times(\hat{n}) &= \hat{l}_a \hat{m}_b + \hat{m}_a \hat{l}_b, \end{aligned} \quad (3.2)$$

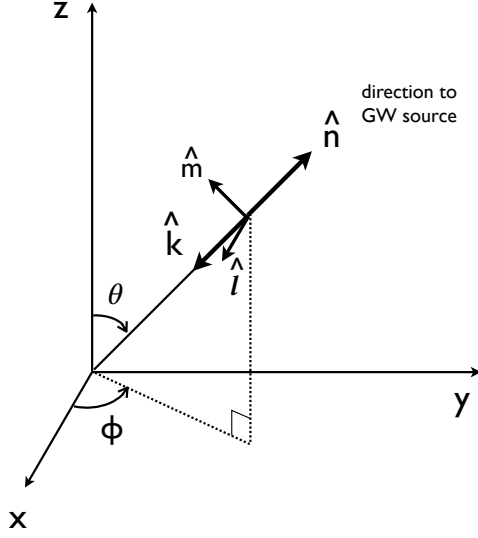


Figure 9: Coordinate system and unit vectors used in the plane-wave expansion of a GWB.

where \hat{l} , \hat{m} are any two orthogonal unit vectors in the plane orthogonal to \hat{n} . Typically, for stochastic background analyses, we take \hat{l} , \hat{m} to be proportional to the standard angular unit vectors tangent to the sphere, so that $\{\hat{k}, \hat{l}, \hat{m}\}$ is a right-handed system (Figure 9):

$$\begin{aligned}\hat{k} &= -\sin \theta \cos \phi \hat{x} - \sin \theta \sin \phi \hat{y} - \cos \theta \hat{z} = -\hat{r}, \\ \hat{l} &= +\sin \phi \hat{x} - \cos \phi \hat{y} = -\hat{\phi}, \\ \hat{m} &= -\cos \theta \cos \phi \hat{x} - \cos \theta \sin \phi \hat{y} + \sin \theta \hat{z} = -\hat{\theta}.\end{aligned}\quad (3.3)$$

For analyzing deterministic sources that have a symmetry axis (e.g., the angular momentum vector for binary inspiral), one takes \hat{l} and \hat{m} to be rotated relative to $-\hat{\phi}$ and $-\hat{\theta}$, where the rotation angle is the *polarization angle* of the source.

3.2 Ensemble averages

The quantities $h_A(f, \hat{n})$ are the Fourier coefficients of the plane wave expansion. Since the metric perturbations for a stochastic background are random variables, so too are the Fourier coefficients. The probability distributions of the Fourier coefficients thus define the statistical properties of the background.

Without loss of generality, we can assume that the expected value of the Fourier coefficients is zero—i.e.,

$$\langle h_A(f, \hat{n}) \rangle = 0, \quad (3.4)$$

where angle brackets denote *ensemble average* over different realizations of the background. (The different realizations could be thought of as the different backgrounds observed by different spatially-located observers in a homogeneous and isotropic universe.) The second-order moments (i.e., quadratic expectation values) specify possible correlations between the Fourier coefficients. For example, if the background is *unpolarized, stationary, and isotropic*, then

$$\langle h_A(f, \hat{n}) h_{A'}^*(f', \hat{n}') \rangle = \frac{1}{16\pi} S_h(f) \delta(f - f') \delta_{AA'} \delta^2(\hat{n}, \hat{n}'), \quad (3.5)$$

where $S_h(f)$ is the *strain power spectral density* of the background, having units of strain² Hz⁻¹. The fact that the RHS is proportional to $\delta(f - f')$ is a consequence of the assumption of *stationarity*—i.e., that there is no preferred origin of time. That the RHS depends on the polarization indices only via $\delta_{AA'}$ is a consequence of the background being unpolarized—i.e., the + and \times polarization components are statistically equivalent and uncorrelated with one another. Similarly, the dependence on sky directions only via $\delta(\hat{n}, \hat{n}')$ is a consequence of isotropy—i.e., that the power in the GWB has no preferred direction on the sky.

If we drop the last assumption, allowing the background to be *anisotropic*, then the quadratic expectation values become

$$\langle h_A(f, \hat{n}) h_{A'}^*(f', \hat{n}') \rangle = \frac{1}{4} \mathcal{P}(f, \hat{n}) \delta(f - f') \delta_{AA'} \delta^2(\hat{n}, \hat{n}'), \quad (3.6)$$

where

$$S_h(f) = \int d^2\Omega_{\hat{n}} \mathcal{P}(f, \hat{n}). \quad (3.7)$$

Here $\mathcal{P}(f, \hat{n})$ is the strain power spectral density per unit solid angle, units strain² Hz¹ sr⁻¹.

For *Gaussian* backgrounds, all cubic and higher-order moments are either identically zero or can be written in terms of the second-order moments. Thus, the quadratic expectation values of the Fourier coefficients completely characterize the statistical properties of a Gaussian-distributed background.

3.3 Energy density spectrum in gravitational waves

As mentioned above, $S_h(f)$ is the strain power spectral density of the GWB. It can be related to the (normalized) *energy density spectrum*

$$\Omega_{\text{gw}}(f) \equiv \frac{1}{\rho_c} \frac{d\rho_{\text{gw}}}{d \ln f} = \frac{f}{\rho_c} \frac{d\rho_{\text{gw}}}{df}, \quad (3.8)$$

where $d\rho_{\text{gw}}$ is the energy density in gravitational waves contained in the frequency interval f to $f + df$, and $\rho_c \equiv 3H_0^2 c^2 / 8\pi G$ is the *critical* energy density (that needed to just close the universe today). The result is

$$S_h(f) = \frac{3H_0^2}{2\pi^2} \frac{\Omega_{\text{gw}}(f)}{f^3}, \quad (3.9)$$

which makes use of the relation

$$\rho_{\text{gw}} = \frac{c^2}{32\pi G} \langle \dot{h}_{ab}(t, \vec{x}) \dot{h}^{ab}(t, \vec{x}) \rangle, \quad (3.10)$$

which gives the energy density in gravitational waves in terms of the quadratic expectation values of the metric perturbations. You are asked in Exercise 2 to derive (3.9); to do so, you will also need to use the plane-wave expansion (3.1) and the quadratic expectation values (3.5 or 3.6).

In addition to $S_h(f)$ and $\Omega_{\text{gw}}(f)$, one sometimes describes the strength of a GWB in terms of the (dimensionless) *characteristic strain* $h_c(f)$ defined by

$$h_c(f) = \sqrt{f S_h(f)}. \quad (3.11)$$

For backgrounds described by a power-law dependence on frequency,³

$$h_c(f) = A_\alpha \left(\frac{f}{f_{\text{ref}}} \right)^\alpha \Leftrightarrow \Omega_{\text{gw}}(f) = \Omega_\beta \left(\frac{f}{f_{\text{ref}}} \right)^\beta, \quad (3.12)$$

³There is no sum over α or β in the following expressions.

where α and β are spectral indices, and A_α and Ω_β are the amplitudes of the characteristic strain and energy density spectrum, respectively, at some reference frequency $f = f_{\text{ref}}$. Using the above definitions and relationships between $\Omega_{\text{gw}}(f)$, $S_h(f)$, and $h_c(f)$, we have

$$\Omega_\beta = \frac{2\pi^2}{3H_0^2} f_{\text{ref}}^2 A_\alpha^2, \quad \beta = 2\alpha + 2. \quad (3.13)$$

For standard inflationary backgrounds, $\Omega_{\text{gw}}(f) = \text{const}$, for which $\beta = 0$ and $\alpha = -1$. For GWBs associated with binary inspiral, $\Omega_{\text{gw}}(f) \propto f^{2/3}$ (as we shall show below), for which $\beta = 2/3$ and $\alpha = -2/3$. This last dependence is valid for both compact binary coalescences consisting of neutron stars and/or stellar-mass black holes (relevant for advanced LIGO, Virgo, etc.), and also for inspirals of supermassive black-holes (SMBHs) in the centers of distant galaxies (relevant for pulsar timing searches).

3.4 Calculating $\Omega_{\text{gw}}(f)$ for an astrophysically-generated background

There is a relatively simple formula for calculating the energy density spectrum $\Omega_{\text{gw}}(f)$ produced by a collection of discrete astrophysical GW sources distributed throughout the universe[1]:

$$\Omega_{\text{gw}}(f) = \frac{1}{\rho_c} \int_0^\infty dz n(z) \frac{1}{1+z} \left(f_s \frac{dE_{\text{gw}}}{df_s} \right) \Big|_{f_s=f(1+z)}. \quad (3.14)$$

We will call this the “Phinney formula”, since it was first written down by E.S. Phinney in an unpublished paper in 2001. For this expression, one needs only the comoving number density of sources $n(z)$ as a function of the cosmological redshift z , and the energy spectrum of an individual source dE_{gw}/df_s as measured in its rest frame. The source frame frequency f_s is related to the observed (present-day) frequency f via $f_s = f(1+z)$. The factor of $1/(1+z)$ in the integrand is needed to redshift the energy measured in the source frame to that measured today.

The above relationship can also be written in terms of the comoving rate density $R(z)$, which is related to the comoving number density $n(z)$ via

$$n(z) dz = R(z) |dt|_{t=t(z)}. \quad (3.15)$$

The result is

$$\Omega_{\text{gw}}(f) = \frac{f}{\rho_c H_0} \int_0^\infty dz R(z) \frac{1}{(1+z)E(z)} \left(\frac{dE_{\text{gw}}}{df_s} \right) \Big|_{f_s=f(1+z)}, \quad (3.16)$$

where

$$E(z) \equiv \sqrt{\Omega_m(1+z)^3 + \Omega_\Lambda} \quad (3.17)$$

is a cosmological factor that arises when evaluating dt/dz . Ω_m and Ω_Λ are the fractional energy densities for matter (ordinary baryonic matter plus dark matter) and dark energy, with numerical values roughly equal to 0.30 and 0.70, respectively. Exercise 3 asks you to prove this “rate-version” of the Phinney formula, filling in some of the cosmology-related details.

3.4.1 Example: $\Omega_{\text{gw}}(f)$ for binary inspiral

To illustrate the Phinney formula in action, we will verify the $\Omega_{\text{gw}}(f) \propto f^{2/3}$ power-law dependence for binary inspiral, which we stated without proof at the end of Section 3.3. Since we are interested here only in the frequency dependence of $\Omega_{\text{gw}}(f)$, all we need to calculate is the energy spectrum dE_{gw}/df_s for a single binary system.

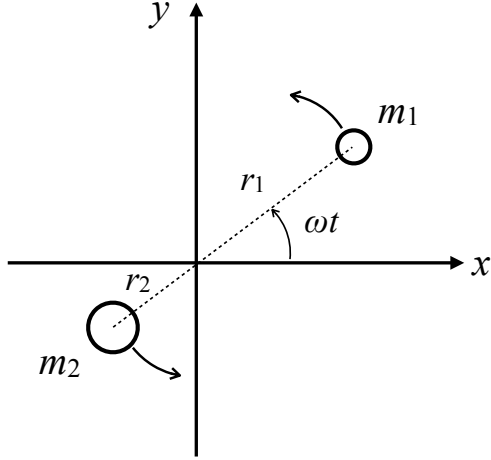


Figure 10: Two masses m_1 , m_2 in orbit around their common center of mass.

So let us consider two masses, m_1 and m_2 , in orbit around their common center of mass (Figure 10). We make the standard definitions

$$r \equiv r_1 + r_2, \quad M \equiv m_1 + m_2, \quad \mu \equiv \frac{m_1 m_2}{m_1 + m_2} \quad (3.18)$$

of the *relative separation*, *total mass*, and *reduced mass* of the system. In terms of these quantities, Kepler's third law and the total orbital energy of the system can be written as

$$\omega^2 r^3 = GM, \quad E_{\text{orb}} = -\frac{GM\mu}{2r}. \quad (3.19)$$

The power emitted in gravitational waves comes from the orbital energy

$$\frac{dE_{\text{gw}}}{dt} = -\frac{dE_{\text{orb}}}{dt}, \quad (3.20)$$

which implies that the energy spectrum is given by

$$\frac{dE_{\text{gw}}}{df_s} = \frac{dt}{df_s} \frac{dE_{\text{gw}}}{dt} = -\frac{dt}{df_s} \frac{dE_{\text{orb}}}{dt}. \quad (3.21)$$

It is now a relatively simple matter to evaluate the RHS of the last expression, using Kepler's law to replace all occurrences of r and \dot{r} with expressions involving ω and $\dot{\omega}$. The final result is

$$\frac{dE_{\text{gw}}}{df_s} \sim \mathcal{M}_c^{5/3} f_s^{-1/3}, \quad \mathcal{M}_c^{5/3} \equiv M^{2/3} \mu, \quad (3.22)$$

where \mathcal{M}_c is the *chirp mass* of the system, and where we have ignored all numerical factors. Note that we also replaced the orbital angular frequency $\omega \equiv 2\pi f_{\text{orb}}$ by the GW frequency $f_s = 2f_{\text{orb}}$, with the factor of 2 arising for quadrupolar radiation in general relativity. Returning now to (3.16), we substitute $f_s = (1+z)f$ and multiply by the factor of f outside the integral to get $\Omega_{\text{gw}}(f) \propto f^{2/3}$ as claimed.

4 Correlation methods

As discussed above, a stochastic background of GWs is described by a *random* signal, which looks like noise in a single detector. As such, standard search techniques like *matched filtering*, which correlate the data against known, deterministic waveforms (e.g., BBH chirps) won't work when trying to detect a GWB. Instead, we have to consider other possibilities: (i) One possibility is to know the noise sources in our GW detector well enough (in both amplitude and spectral shape) that we can attribute any unexpected excess "noise" to a GWB. (This was basically how Penzias and Wilson initially detected the CMB; they saw an excess noise temperature of $\sim 3.5^\circ$ K in their radio antenna that they could not attribute to any other noise source.) (ii) Another possibility is to use data from multiple detectors. Then we can look for evidence of a common disturbance in the multiple data streams consistent with each detector's response to gravitational waves.

Currently, (i) is not an option for ground-based interferometers since the noise sources are not known at the level needed to attribute any observed excess power to gravitational waves. But (ii) is an option as LIGO consists of two detectors, one in Hanford, WA, the other in Livingston, LA. Virgo, in Italy, provides a third detector, and soon we will have two more large-scale interferometers in Japan and India. Cross-correlating data from multiple detectors works for detecting a GWB since, even though the signal is random, it is the *same* signal in the different detectors (modulo the physical separation and relative orientation of the detectors). In effect, the random output of one detector is used as a template for the data in another detector. As we shall see below, the signal-to-noise ratio of the cross-correlation grows like the square-root of the observation time. Thus, although the GWB might be weak relative to the noise, it can still be extracted from a cross-correlation measurement if it is observed for a long enough period of time.

4.1 Basic idea

To illustrate the basic idea behind cross-correlation, we will consider first the simplest possible scenario—i.e., a single sample of data from two colocated and coaligned detectors:

$$\begin{aligned} d_1 &= h + n_1, \\ d_2 &= h + n_2. \end{aligned} \tag{4.1}$$

Here h denotes the common GW signal component, and n_1, n_2 denote the corresponding instrumental noise components. Cross-correlating the data for this case amounts to simply taking the product of the two data samples, $\hat{C}_{12} \equiv d_1 d_2$. The expected value of the cross-correlation is

$$\langle \hat{C}_{12} \rangle = \langle d_1 d_2 \rangle = \langle h^2 \rangle + \cancel{\langle h n_2 \rangle}^0 + \cancel{\langle n_1 h \rangle}^0 + \langle n_1 n_2 \rangle, \tag{4.2}$$

where we $\langle h n_2 \rangle = 0 = \langle n_1 h \rangle$, since the GW signal and instrumental noise are not correlated with one another. If we further assume that the noise in the two detectors is *uncorrelated* (which is a good valid assumption if the detectors are widely separated⁴), then $\langle n_1 n_2 \rangle = 0$, leaving

$$\langle \hat{C}_{12} \rangle = \langle h^2 \rangle \equiv S_h, \tag{4.3}$$

which is just the variance (i.e., power) in the GW signal.

⁴Note that global magnetic fields, e.g., Schumann resonances, *can* produce environmental correlations in widely separated detectors.

4.2 Extension to multiple data samples

The above analysis can be easily extended to the case of multiple samples:

$$\begin{aligned} d_{1i} &= h_i + n_{1i}, \\ d_{2i} &= h_i + n_{2i}, \end{aligned} \quad (4.4)$$

where $i = 1, 2, \dots, N$. As before, we will assume that the two detectors are coincident and coaligned, and that the noise in the two detectors are uncorrelated with the GW signal and with one another

$$\langle n_{1i}h_j \rangle = 0, \quad \langle n_{2i}h_j \rangle = 0, \quad \langle n_{1i}n_{2j} \rangle = 0. \quad (4.5)$$

We will also assume that the GWB and detector noise are both *white*, which means

$$\langle h_ih_j \rangle = S_h \delta_{ij}, \quad \langle n_{1i}n_{1j} \rangle = S_{n_1} \delta_{ij}, \quad \langle n_{2i}n_{2j} \rangle = S_{n_2} \delta_{ij}, \quad (4.6)$$

where S_h , S_{n_1} , S_{n_2} are the variances (i.e., power) in the GW signal and detector noise, respectively. For this case, our cross-correlation statistic is the average of the products of the individual data samples

$$\hat{S}_h \equiv \hat{C}_{12} \equiv \frac{1}{N} \sum_{i=1}^N d_{1i}d_{2i}, \quad (4.7)$$

which, as we shall see below, is again an estimator of the power in the GWB (hence the “hat” (^) over the S_h on the LHS of this equation).

Using the above definitions and quadratic expectation values, it is easy to show that

$$\mu \equiv \langle \hat{C}_{12} \rangle = \frac{1}{N} \sum_{i=1}^N \langle d_{1i}d_{2i} \rangle = \frac{1}{N} \sum_{i=1}^N \langle h_i^2 \rangle = S_h. \quad (4.8)$$

Thus, the cross-correlation statistic \hat{C}_{12} is an (unbiased) estimator of the GW power S_h . The variance in this estimator can be calculated via

$$\sigma^2 \equiv \langle \hat{C}_{12}^2 \rangle - \langle \hat{C}_{12} \rangle^2 = \left(\frac{1}{N} \right)^2 \sum_{i=1}^N \sum_{j=1}^N (\langle d_{1i}d_{2i}d_{1j}d_{2j} \rangle - \langle d_{1i}d_{2i} \rangle \langle d_{1j}d_{2j} \rangle). \quad (4.9)$$

To evaluate the RHS of the above equation, we make use of the identity

$$\langle abcd \rangle = \langle ab \rangle \langle cd \rangle + \langle ac \rangle \langle bd \rangle + \langle ad \rangle \langle bc \rangle, \quad (4.10)$$

which is valid for zero-mean Gaussian random variables. Using this identity and the quadratic expectation values between the signal and noise, we end up with

$$\sigma^2 = \frac{1}{N} (S_1 S_2 + S_h^2) \quad (4.11)$$

where

$$S_1 \equiv S_{n_1} + S_h, \quad S_2 \equiv S_{n_2} + S_h, \quad (4.12)$$

are the total power in the detector output (consisting of both signal and noise power). Since the power in the GWB is expected to be weak compared to the detector noise, the variance can be approximated as $\sigma^2 \simeq S_1 S_2 / N$, for which the expected signal-to-noise ratio is given by

$$\rho \equiv \frac{\mu}{\sigma} \simeq \frac{S_h}{\sqrt{S_1 S_2 / N}} \simeq \sqrt{N} \frac{S_h}{S_n}, \quad (4.13)$$

where $\sqrt{S_1 S_2} \simeq \sqrt{S_{n_1} S_{n_2}} \equiv S_n$. This result verifies the statement made earlier that the signal-to-noise ratio for a cross-correlation measurement grows like the square-root of the observation time (in this case, the total number of samples).

4.3 Optimal filtering

To handle the case of physically-separated and misaligned detectors, we need to include the non-trivial response of a GW detector to a GWB. We will do this in more detail in Sections 6 and 7. For now, we simply state without proof that the correlated response of physically separated and misaligned detectors to a GWB is represented by the so-called *overlap function* (or overlap reduction function), denoted $\Gamma_{12}(f)$, which relates the strain power in the GWB, $S_h(f)$, to the cross-correlated signal power in two detectors, i.e., $C_{12}(f) = \Gamma_{12}(f)S_h(f)$. In terms of the quadratic expectation values of the GW signal in the two detectors⁵:

$$\langle \tilde{h}_1(f)\tilde{h}_2^*(f') \rangle = \frac{1}{2}\delta(f-f')\Gamma_{12}(f)S_h(f), \quad (4.14)$$

where $\tilde{h}_1(f)$, $\tilde{h}_2(f)$ denote the Fourier transforms of GW signal components $h_1(t)$, $h_2(t)$ in the two detectors. For comparison, the (auto-correlated) power spectra of the detector noise $P_{n_1}(f)$, $P_{n_2}(f)$ are defined in terms of the noise components $\tilde{n}_1(f)$, $\tilde{n}_2(f)$ via:

$$\begin{aligned} \langle \tilde{n}_1(f)\tilde{n}_1^*(f') \rangle &= \frac{1}{2}\delta(f-f')P_{n_1}(f), \\ \langle \tilde{n}_2(f)\tilde{n}_2^*(f') \rangle &= \frac{1}{2}\delta(f-f')P_{n_2}(f), \end{aligned} \quad (4.15)$$

and the cross-correlated noise is assumed to be zero:

$$\langle \tilde{n}_1(f)\tilde{n}_2^*(f') \rangle = 0. \quad (4.16)$$

Plots of $\Gamma_{12}(f)$ for the LIGO Hanford and LIGO Livingston interferometers, and for LIGO Hanford and Virgo interferometers can be found in Section 7.

Given the above definitions, we can now ask the question: what is the optimal way to correlate data from two physically separated and possibly mis-aligned detectors to search for an isotropic GWB? To answer this question, we start by forming the generic cross-correlation

$$\hat{C}_{12} = \int_{-T/2}^{T/2} dt \int_{-T/2}^{T/2} dt' d_1(t)d_2(t)Q(t,t'), \quad (4.17)$$

where $Q(t,t')$ is an a priori arbitrary filter function and T is the observation time. For stationary data, $Q(t,t')$ should depend only on the difference between the two time arguments, $\Delta t \equiv t - t'$, so that $Q(t,t') \equiv Q(t - t')$. In the Fourier domain, we can then write

$$\hat{C}_{12} \simeq \int_{-\infty}^{\infty} df \int_{-\infty}^{\infty} df' \delta_T(f-f')\tilde{d}_1(f)\tilde{d}_2(f')\tilde{Q}^*(f'), \quad (4.18)$$

where $\tilde{Q}(f)$ is the Fourier transform of $Q(\Delta t)$, and $\delta_T(f-f')$ is a finite-time version of the Dirac delta function defined by $\delta_T(f-f') \equiv T \text{sinc}(f-f')$, where $\text{sinc } x \equiv \sin x/x$.

To proceed further we need to define what we mean by *optimal*. A natural criterion in this context is to *maximize the expected signal-to-noise ratio* of \hat{C}_{12} for a GWB with a fixed spectral shape $H(f)$. (The expected signal-to-noise ratio is defined as in the previous section $\rho \equiv \mu/\sigma$, where

⁵The factor of 1/2 is included on the RHS so that the power spectrum is *one-sided*. In other words, the total cross-correlated power in the GWB is given by the integral of $\Gamma_{12}(f)S_h(f)$ over just the *positive* frequencies. The factor of $\delta(f-f')$ is a consequence of stationarity.

$\mu \equiv \langle \hat{C}_{12} \rangle$ and $\sigma^2 \equiv \langle \hat{C}_{12}^2 \rangle - \langle \hat{C}_{12} \rangle^2$.) As you are asked to show in Exercise 4, this maximization condition determines the form of the filter function $\tilde{Q}(f)$ up to an overall normalization:

$$\tilde{Q}(f) \propto \frac{\Gamma_{12}(f)H(f)}{P_1(f)P_2(f)}, \quad (4.19)$$

where $P_1(f)$, $P_2(f)$ are the total power in the two detectors—i.e., $P_1(f) = P_{n1}(f) + P_{\text{gw}}(f)$, $P_2(f) = P_{n2}(f) + P_{\text{gw}}(f)$, which are approximately equal to $P_{n1}(f)$, $P_{n2}(f)$ assuming that the GW signal is weak compared to the detector noise. Note that the numerator of $\tilde{Q}(f)$ is proportional to the expected value of the cross-correlated data in the frequency domain, while the denominator basically deweights the correlation when the detector noise is large. The dependence of $\tilde{Q}(f)$ on the spectral shape $H(f)$ means that the optimal filter is tuned to a particular GWB.

The overall normalization of the optimal filter $\tilde{Q}(f)$ is not determined by the maximization condition, since the normalization factor cancels out in the calculation of the signal-to-noise ratio $\rho = \mu/\sigma$. Typically, one uses this freedom in the choice of normalization factor to set the expected value μ equal to the amplitude of the background—i.e., $\mu = \Omega_{\text{gw}}(f_{\text{ref}})$. In other words, the measured value of the cross-correlation, \hat{C}_{12} , is a *point estimate* of $\Omega_{\text{gw}}(f_{\text{ref}})$.

5 Optimal filtering applied to some simple examples

We now apply the above correlation methods to some simple examples involving simulated data.⁶ We will consider three different GWBs injected into uncorrelated, white detector noise in two coincident and coaligned detectors: (i) a white GWB, (ii) a confusion-limited BNS GWB, and (iii) a two-component GWB, formed from the superposition of the GWBs from (i) and (ii). The simulated time-domain data for the three different cases are shown in Figure 11. Recall that a white GWB has spectral shape $H(f) = 1$, while a confusion-limited background of BNS has spectral shape $H(f) = (f/f_{\text{ref}})^{-7/3}$ (see Figure 7).

5.1 Single-component analyses

For example (i), we find that the measured and injected values of the amplitude of the GWB agree to 3.5%, which is within $1-\sigma$. The corresponding optimally-filtered signal-to-noise ratio is $\rho = 2.9$. For example (ii), the measured and injected values of the amplitude of the GWB agree to 2.7%, which again is within $1-\sigma$. The corresponding optimally-filtered signal-to-noise ratio for this case is $\rho = 12$. Note that even though the overall amplitude of the background is noticeably smaller for the confusion-limited BNS GWB, the signal-to-noise ratio is considerably larger (12 versus 2.9). This is because the spectrum of the GW signal differs in this case from that of the detector noise, which helps in distinguishing the signal and noise components.

Finally for example (iii), if we filter the data for the two components separately, we overestimate the amplitude of the white GWB component by 48%, which is greater than $1-\sigma$, and overestimate the amplitude of the BNS GWB by 6.9%, which is within $1-\sigma$. Basically, filtering the data for each GWB component separately typically leads to *overestimates* of the amplitudes of the individual components but *underestimates* the error bars. The overestimates arise since the other GWB component also contributes to the correlated signal.

⁶These are *toy model* simulations, whose sole purpose is to illustrate how optimal filtering works. The amplitude and duration of the simulated data are not meant to be representative of real searches for GWBs.

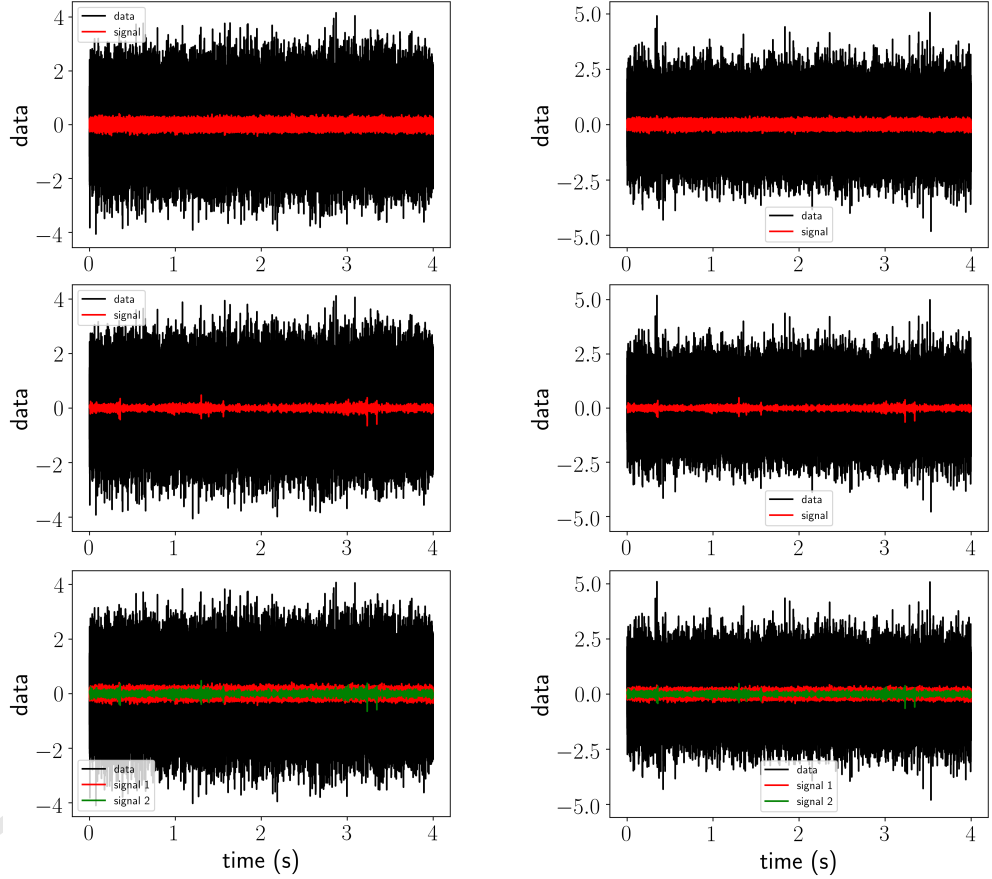


Figure 11: Simulated time-domain data for the three different cases discussed in the main text: (top row) a white GWB in uncorrelated, white detector noise, (middle row) a confusion-limited BNS GWB in uncorrelated, white detector noise, (bottom row) a two-component GWB formed from the superposition of the GWBs from the top two rows in uncorrelated, white detector noise.

5.2 Multi-component analysis

To better extract the amplitudes of the individual components for example (iii), we need to go beyond the simple one-component filtering model, enlarging our signal model to allow for a superposition of multiple GWB components. (We will explain this in more detail below.) Doing so allows us to extract the amplitude of the white GWB component to 7.3%, corresponding to a signal-to-noise ratio of 1.4, and extract the amplitude of the BNS GWB component to 3.8%, corresponding to a signal-to-noise ratio of 6.0. This *joint* analysis for the two components properly takes into account the *covariance* between the spectral shapes of the two components [?].

To see how this joint analysis works in more detail, we will write down a likelihood function for the data

$$\hat{C}_{12}(f) \equiv \frac{2}{T} \tilde{d}_1(f) d_2(f). \quad (5.1)$$

The expected value of this correlated data is

$$\langle \hat{C}_{12}(f) \rangle = \sum_{\alpha} \Gamma_{12}(f) H_{\alpha}(f) \equiv \sum_{\alpha} M_{\alpha}(f) A_{\alpha}, \quad (5.2)$$

where $H_{\alpha}(f)$ are the different spectral shapes with amplitudes A_{α} . The covariance matrix of the data is given by

$$\begin{aligned} N_{12}(f, f') &\equiv \langle \hat{C}_{12}(f) \hat{C}_{12}^*(f') \rangle - \langle \hat{C}_{12}(f) \rangle \langle \hat{C}_{12}^*(f') \rangle \\ &\simeq \delta_{ff'} P_1(f) P_2(f) \end{aligned} \quad (5.3)$$

in the weak-signal approximation. The likelihood function is then
that is not consistent with uncorrelated noise.

For the two-component background example, one should instead filter for both components
imagine filtering

6 Non-trivial detector response

7 Non-trivial correlations

8 What to do in the absence of correlations?

9 Searching for the background of binary black-hole mergers

10 Exercises

A more detailed description of the suggested exercises.

1. Rate estimate of stellar-mass binary black hole mergers:

Estimate the total rate (number of events per time) of stellar-mass binary black hole mergers throughout the universe by multiplying LIGO's O1 local rate estimate $R_0 \sim 10 - 200 \text{ Gpc}^{-3} \text{ yr}^{-1}$ by the comoving volume out to some large redshift, e.g., $z = 10$. (For this calculation you can ignore any dependence of the rate density with redshift.) You should find a merger rate of ~ 1 per minute to a few per hour.

Hint: You will need to do numerically evaluate the following integral for proper distance today as a function of source redshift:

$$d_0(z) = \frac{c}{H_0} \int_0^z \frac{dz'}{E(z')} , \quad E(z) \equiv \sqrt{\Omega_m(1+z)^3 + \Omega_\Lambda} , \quad (10.1)$$

with

$$\Omega_m = 0.31 , \quad \Omega_\Lambda = 0.69 , \quad H_0 = 68 \text{ km s}^{-1} \text{ Mpc}^{-1} . \quad (10.2)$$

Doing that integral, you should find what's shown in Figure 12, which you can then evaluate at $z = 10$ to convert R_0 (number of events per comoving volume per time) to total rate (number of events per time) for sources out to redshift $z = 10$.

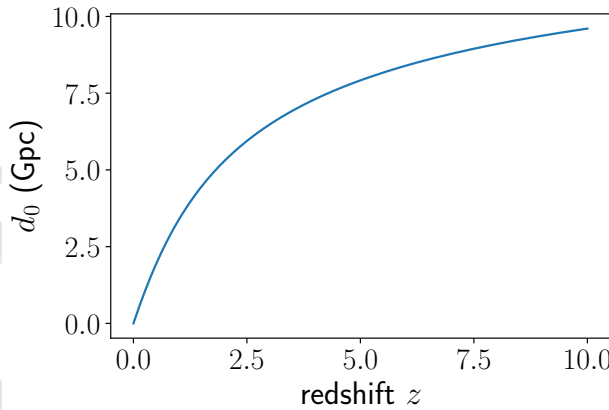


Figure 12

2. Relating $S_h(f)$ and $\Omega_{\text{gw}}(f)$:

Derive the relationship

$$S_h(f) = \frac{3H_0^2}{2\pi^2} \frac{\Omega_{\text{gw}}(f)}{f^3} \quad (10.3)$$

between the strain power spectral density $S_h(f)$ and the dimensionless fractional energy density spectrum $\Omega_{\text{gw}}(f)$. (*Hint:* You will need to use the various definitions of these quantities and also

$$\rho_{\text{gw}} = \frac{c^2}{32\pi G} \langle \dot{h}_{ab}(t, \vec{x}) \dot{h}^{ab}(t, \vec{x}) \rangle , \quad (10.4)$$

which expresses the energy-density in gravitational-waves to the metric perturbations $h_{ab}(t, \vec{x})$.)

3. Cosmology and the “Phinney formula” for astrophysical backgrounds:

(a) Using the Friedmann equation

$$\left(\frac{\dot{a}}{a}\right)^2 = H_0^2 \left(\frac{\Omega_m}{a^3} + \Omega_\Lambda \right) \quad (10.5)$$

for a spatially-flat FRW spacetime with matter and cosmological constant, and the relationship

$$1+z = \frac{1}{a(t)}, \quad a(t_0) \equiv 1 \quad (t_0 \equiv \text{today}), \quad (10.6)$$

between redshift z and scale factor $a(t)$, derive

$$\frac{dt}{dz} = -\frac{1}{(1+z)H_0E(z)}, \quad E(z) = \sqrt{\Omega_m(1+z)^3 + \Omega_\Lambda}. \quad (10.7)$$

(b) Using this result for dt/dz , show that

$$\Omega_{\text{gw}}(f) = \frac{f}{\rho_c H_0} \int_0^\infty dz R(z) \frac{1}{(1+z)E(z)} \left(\frac{dE_{\text{gw}}}{df_s} \right) \Big|_{f_s=f(1+z)} \quad (10.8)$$

in terms of the rate density $R(z)$ as measured in the source frame (number of events per comoving volume per time interval in the source frame). (*Hint:* The expression for dt/dz from part (a) will allow you to go from the “Phinney formula” for $\Omega_{\text{gw}}(f)$ written in terms of the number density $n(z)$,

$$\Omega_{\text{gw}}(f) = \frac{1}{\rho_c} \int_0^\infty dz n(z) \frac{1}{1+z} \left(f_s \frac{dE_{\text{gw}}}{df_s} \right) \Big|_{f_s=f(1+z)}, \quad (10.9)$$

to one in terms of the rate density $R(z)$, where $n(z) dz = R(z) |dt|_{t=t(z)}$. Note: Both of the above expressions for $\Omega_{\text{gw}}(f)$ assume that there is only one type of source, described by some set of average source parameters. If there is more than one type of source, one must sum the contributions of each source to $\Omega_{\text{gw}}(f)$.)

4. Optimal filtering for the cross-correlation statistic:

Verify the form

$$\tilde{Q}(f) \propto \frac{\Gamma_{12}(f)H(f)}{P_1(f)P_2(f)}, \quad (10.10)$$

of the optimal filter function in the weak-signal limit, where $H(f)$ is the assumed spectral shape of the gravitational-wave background, $\Gamma_{12}(f)$ is the overlap function, and $P_1(f)$, $P_2(f)$ are the power spectral densities of the outputs of the two detectors (which are approximately equal to $P_{n_1}(f)$, $P_{n_2}(f)$, respectively). Recall that the optimal filter $\tilde{Q}(f)$ maximizes the signal-to-noise ratio of the cross-correlation statistic. (*Hint:* Introduce an inner product on the space of functions of frequency $A(f)$, $B(f)$:

$$(A, B) \equiv \int df A(f)B^*(f)P_1(f)P_2(f). \quad (10.11)$$

This inner product has all of the properties of the familiar dot product of vectors in 3-dimensional space. The signal-to-noise ratio of the cross-correlation statistic can be written in terms of this inner product.)

5. Maximum-likelihood estimators for single and multiple parameters:

- (a) Show that the maximum-likelihood estimator \hat{a} of the single parameter a in the likelihood function

$$p(d|a, \sigma) \propto \exp \left[-\frac{1}{2} \sum_{i=1}^N \frac{(d_i - a)^2}{\sigma_i^2} \right] \quad (10.12)$$

is given by the noise-weighted average

$$\hat{a} = \sum_i \frac{d_i}{\sigma_i^2} / \sum_j \frac{1}{\sigma_j^2}. \quad (10.13)$$

- (b) Extend the previous calculation to the likelihood

$$p(d|A, C) \propto \exp \left[-\frac{1}{2} (d - MA)^\dagger C^{-1} (d - MA) \right], \quad (10.14)$$

where $A \equiv A_\alpha$ is a vector of parameters, $C \equiv C_{ij}$ is the noise covariance matrix, and $M \equiv M_{i\alpha}$ is the response matrix mapping A_α to data samples, $MA \equiv \sum_\alpha M_{i\alpha} A_\alpha$. For this more general case you should find:

$$\hat{A} = F^{-1}X, \quad (10.15)$$

where

$$F \equiv M^\dagger C^{-1} M, \quad X \equiv M^\dagger C^{-1} d. \quad (10.16)$$

In general, the matrix F (called the *Fisher* matrix) is not invertible, so some sort of regularization is needed to do the matrix inversion.

6. Timing-residual response for a 1-arm, 1-way detector:

Derive the timing residual response function

$$R^A(f, \hat{n}) = \frac{1}{2} u^a u^b e_{ab}^A(\hat{n}) \frac{1}{i2\pi f} \frac{1}{1 + \hat{n} \cdot \hat{u}} \left[1 - e^{-\frac{i2\pi f L}{c}(1 + \hat{n} \cdot \hat{u})} \right] \quad (10.17)$$

for a single-link (i.e., a one-arm, one-way detector like that for pulsar timing). Here \hat{u} is the direction of propagation of the electromagnetic pulse, and \hat{n} is the direction to the GW source (the direction of wave propagation is $\hat{k} \equiv -\hat{n}$ and the direction to the pulsar is $\hat{p} \equiv -\hat{u}$). The origin of coordinates is taken to be at the position of the detector.

7. Overlap function for colocated electric dipole antennae:

Show that the overlap function for a pair of (short) colocated electric dipole antennae pointing in directions \hat{u}_1 and \hat{u}_2 is given by

$$\Gamma_{12} \propto \hat{u}_1 \cdot \hat{u}_2 \equiv \cos \zeta \quad (10.18)$$

for the case of an unpolarized, isotropic electromagnetic field. (*Hint:* “short” means that the phase of the electric field can be taken to be constant over of the lengths of the dipole antennae, so that the response of antenna $I = 1, 2$ to the field is given by $r_I(t) = \hat{u}_I \cdot \vec{E}(t, \vec{x}_0)$, where \vec{x}_0 is the common location of the two antenna.)

8. Maximum-likelihood estimators for the standard cross-correlation statistic:

Verify that

$$\hat{C}_{11} \equiv \frac{1}{N} \sum_{i=1}^N d_{1i}^2, \quad \hat{C}_{22} \equiv \frac{1}{N} \sum_{i=1}^N d_{2i}^2, \quad \hat{C}_{12} \equiv \frac{1}{N} \sum_{i=1}^N d_{1i}d_{2i} \quad (10.19)$$

are maximum-likelihood estimators of

$$S_1 \equiv S_{n_1} + S_h, \quad S_2 \equiv S_{n_2} + S_h, \quad S_h, \quad (10.20)$$

for the case of N samples of a white GWB in uncorrelated white detector noise, for a pair of colocated and coaligned detectors. Recall that the likelihood function is

$$p(d|S_{n_1}, S_{n_2}, S_h) = \frac{1}{\sqrt{\det(2\pi C)}} \exp \left[-\frac{1}{2} d^T C^{-1} d \right], \quad (10.21)$$

where

$$C = \begin{bmatrix} (S_{n_1} + S_h) \mathbf{1}_{N \times N} & S_h \mathbf{1}_{N \times N} \\ S_h \mathbf{1}_{N \times N} & (S_{n_2} + S_h) \mathbf{1}_{N \times N} \end{bmatrix} \quad (10.22)$$

and

$$d^T C^{-1} d \equiv \sum_{I,J=1}^2 \sum_{i,j=1}^N d_{Ii} (C^{-1})_{Ii, Jj} d_{Jj}. \quad (10.23)$$

9. Derivation of the maximum-likelihood ratio detection statistic:

Verify that twice the log of the maximum-likelihood ratio for the standard stochastic likelihood function goes like the square of the (power) signal-to-noise ratio,

$$2 \ln \Lambda_{\text{ML}}(d) \simeq \frac{\hat{C}_{12}^2}{\hat{C}_{11} \hat{C}_{22}/N}, \quad (10.24)$$

in the weak-signal approximation. (*Hint:* For simplicity, do the calculation in the context of N samples of a white GWB in uncorrelated white detector noise, for a pair of colocated and coaligned detectors, using the results of Exercise 8.)

10. Standard cross-correlation likelihood by marginalizing over stochastic signal prior:

Derive the standard form of the likelihood function for stochastic background searches

$$p(d|S_{n_1}, S_{n_2}, S_h) = \frac{1}{\sqrt{\det(2\pi C)}} \exp \left[-\frac{1}{2} \sum_{I,J=1}^2 d_I (C^{-1})_{IJ} d_J \right], \quad (10.25)$$

where

$$C \equiv \begin{bmatrix} S_{n_1} + S_h & S_h \\ S_h & S_{n_2} + S_h \end{bmatrix}, \quad (10.26)$$

by marginalizing

$$p_n(d - h|S_{n_1}, S_{n_2}) = \frac{1}{2\pi\sqrt{S_{n_1}S_{n_2}}} \exp \left[-\frac{1}{2} \left\{ \frac{(d_1 - h)^2}{S_{n_1}} + \frac{(d_2 - h)^2}{S_{n_2}} \right\} \right] \quad (10.27)$$

over the signal samples h for the *stochastic* signal prior

$$p(h|S_h) = \frac{1}{\sqrt{2\pi S_h}} \exp\left[-\frac{1}{2} \frac{h^2}{S_h}\right]. \quad (10.28)$$

In other words, show that

$$p(d|S_{n_1}, S_{n_2}, S_h) = \int_{-\infty}^{\infty} dh p_n(d - h|S_{n_1}, S_{n_2}) p(h|S_h). \quad (10.29)$$

(*Hint:* You'll have to complete the square in the argument of the exponential in the marginalization integral.)

References

- [1] Phinney, E.S., “A practical theorem on gravitational wave backgrounds” (2001). [arXiv:0108028 [astro-ph.IM]].
- [2] Romano, Joseph D. and Cornish, Neil. J., “Detection methods for stochastic gravitational-wave backgrounds: a unified treatment”, *Living Reviews in Relativity*, **20**(1), 2 (Apr 04, 2017). [DOI]URL:
<https://doi.org/10.1007/s41114-017-0004-1>.
- [3] Smith, Rory and Thrane, Eric, “Optimal Search for an Astrophysical Gravitational-Wave Background”, *Phys. Rev. X*, **8**, 021019 (Apr 2018). [DOI]URL:
<https://link.aps.org/doi/10.1103/PhysRevX.8.021019>.